

Published in final edited form as:

Cancer Res. 2015 April 1; 75(7): 1216–1224. doi:10.1158/0008-5472.CAN-14-1997.

Exploring the Biomechanical Properties of Brain Malignancies and their Pathological Determinants *In Vivo* with Magnetic Resonance Elastography

Yann Jamin^{#1}, Jessica K.R. Boulton^{#1}, Jin Li^{#1}, Sergey Popov^{2,3}, Philippe Garteiser⁴, Jose L. Ulloa⁵, Craig Cummings¹, Gary Box³, Suzanne A. Eccles³, Chris Jones^{2,3}, John C. Waterton⁶, Jeffrey C. Bamber¹, Ralph Sinkus^{7,‡}, and Simon P. Robinson^{1,‡}

¹Division of Radiotherapy & Imaging, The Institute of Cancer Research and Royal Marsden NHS Trust, London, United Kingdom.

²Division of Molecular Pathology, The Institute of Cancer Research, London, United Kingdom.

³Division of Cancer Therapeutics, The Institute of Cancer Research, London, United Kingdom.

⁴INSERM U1149, CRI, Centre de Recherche sur l'Inflammation, Paris, France.

⁵Bioxydyn Ltd, Manchester, United Kingdom.

⁶Personalised Healthcare and Biomarkers, AstraZeneca, Alderley Park, Macclesfield, Cheshire, United Kingdom.

⁷BHF Centre of Excellence, Division of Imaging Sciences and Biomedical Engineering, King's College London, King's Health Partners, St. Thomas' Hospital, London, United Kingdom.

These authors contributed equally to this work.

Abstract

Malignant tumors are typically associated with altered rigidity relative to normal host tissue. Magnetic resonance elastography (MRE) enables the noninvasive quantitation of the mechanical properties of deep-seated tissue following application of an external vibrational mechanical stress to that tissue. In this preclinical study, we used MRE to quantify (kPa) the elasticity modulus G_d and viscosity modulus G_v of three intracranially implanted glioma and breast metastatic tumor models. In all these brain tumors, we found a notable softness characterized by lower elasticity and viscosity than normal brain parenchyma, enabling their detection on G_d and G_v parametric maps. The most circumscribed tumor (U-87 glioma) was the stiffest whereas the most infiltrative tumor (MDA-MB-231 metastatic breast carcinoma) was the softest. Tumor cell density and microvessel density correlated positively with elasticity and viscosity significantly, whereas there was no association with the extent of collagen deposition or myelin fiber entrapment. In

Corresponding author: Dr. Yann Jamin, Cancer Research UK Cancer Imaging Centre, Division of Radiotherapy and Imaging, The Institute of Cancer Research, London and Royal Marsden NHS Foundation, 15 Cotswold Road, Sutton, Surrey, SM2 5NG, United Kingdom. Yann.Jamin@icr.ac.uk, Tel: +44 20 8661 3774, Fax: +44 20 8661 0846.

[‡]R.S., S.P.R. contributed equally to this work

Conflict of interest: The authors have no conflict of interest to disclose. John Waterton has employment, stock and stock options in AstraZeneca, a for-profit company engaged in the discovery, development, manufacture and marketing of proprietary therapeutics. He does not consider that this creates any conflict of interest with the subject-matter of the manuscript.

conclusion, while malignant tumors tend to exhibit increased rigidity, intracranial tumors presented as remarkably softer than normal brain parenchyma. Our findings reinforce the case for MRE use in diagnosing and staging brain malignancies, based on the association of different tumor phenotypes with different mechanical properties.

Keywords

Magnetic Resonance Elastography; Brain tumors; Elasticity; Viscosity; Mechanical properties

Introduction

Altered tissue stiffness through loss of tensional homeostasis is a hallmark of cancer. The changes that occur at a cellular level during oncogenesis and tumor progression cause dramatic changes in the architecture and mechanical properties of both the tumor and surrounding host tissue. Malignant tumors have been typically associated with increased tissue rigidity relative to the normal host tissue, which may influence therapeutic response and promote metastasis (1-3) and invasiveness. There is also growing evidence that an increase in local stiffness may promote the malignant transformation of normal cells (4,5).

The morphology of both tumor cells and each component of their microenvironment (vasculature, fibroblast/immune cell infiltration, and extracellular matrix) manifestly shape the macroscopic mechanical properties of each tumor type, and may also define aggressive, invasive, metastatic and resistant phenotypes (6,7). Physical palpation exploits the differences in compliance between tumor and host tissue, and has provided an invaluable, yet limited, diagnostic tool for the detection of malignancies since before the origin of modern medicine.

Diagnostic imaging is an essential tool in the management of patients with brain cancer. MRI has become the methodology of choice due to its exquisite soft tissue image contrast, which enables the visualisation of detailed anatomical features with high resolution. Advanced functional MRI methodologies have improved radiological-based diagnosis of brain tumors, but still demonstrate low specificity. The final diagnosis still relies on pathological examination of the resected tumor or biopsy samples, both obtained at high risk of morbidity. Patients with grade IV malignant glioma only have a median survival of 12-15 months. While low-grade gliomas have a better prognosis, there is, as yet, no assured cure. Patients with brain metastases, which affect up to 40% of patients with metastatic cancer, have a similarly poor prognosis. With new promising targeted strategies for the treatment of patients with brain malignancies has come the unmet need for refined non-invasive imaging strategies that could provide more specific diagnostic, predictive (enabling the stratification of patients who would benefit from the treatment) and prognostic (to determine the potential to achieve favorable clinical outcome) biomarkers.

Elastography is the imaging of the mechanical properties of tissue, which may be accomplished with any conventional anatomical imaging modality such as MRI, ultrasound, X-ray and optical imaging. Magnetic resonance elastography (MRE) is an emerging MRI methodology, which enables the quantitative and non-invasive assessment of tissue

mechanical properties *in vivo*. MRE relies on the ability of MRI to visualise the propagation of low-frequency shear waves, whose characteristics are directly determined by the local viscoelastic properties of the tissue of interest (8). Since low frequency waves can be mechanically applied through the skull, MRE is uniquely positioned to assess the viscoelastic properties of brain tissue *in situ*. MRE has already been successfully implemented in the clinic, in both healthy volunteers and patients with brain tumors (9-12).

In this study, we used MRE to investigate the viscoelastic properties of three intracranially implanted tumors with different infiltrative patterns of growth. Using histopathological correlates, we investigated the physiological and structural determinants of the different viscoelastic properties measured between brain parenchyma and tumors, as well as between different tumor types, and discuss the potential of MRE for the diagnosis and stratification of patients presenting with brain malignancies.

Materials and Methods

Cell Lines

U-87 MG human glioblastoma cells (American Type Culture Collection, LGC Standards, Teddington, UK) engineered to stably express pCDF1-MCS2-EFIPuro-luc, RG2 rat glioma cells (American Type Culture Collection) that stably express pGL4.50[luc2/CMV/hygro] (kind gift from Dr. D. Crichton, Cancer Research Technology, The Beatson Institute for Cancer Research, Glasgow) and luciferase-expressing MDA-MB-231 LM2-4 human triple negative breast carcinoma cells (13) (provided by Dr. R. Kerbel, University of Toronto, Canada) were maintained in Dulbecco's Modified Eagle's Medium supplemented with 10% (v/v) fetal bovine serum (Invitrogen, Life Technologies, Paisley, UK). All cells were tested for mycoplasma at the time of tumor propagation and were found to be negative.

Animals

Six week old female athymic (NCr nu/nu) mice were obtained from Charles River Ltd (Margate, UK). All experiments were performed in accordance with the local ethical review panel, the UK Home Office Animals (Scientific Procedures) Act 1986, the United Kingdom National Cancer Research Institute guidelines for the welfare of animals in cancer research (14) and the ARRIVE (animal research: reporting in vivo experiments) guidelines (15).

Intracranial Injections and Bioluminescence Imaging

U-87 MG (5×10^4), RG2 or MDA-MB-231 cells (5×10^3) were implanted supratentorially in the brains of mice. Animals were anesthetized using 1-2% isoflurane in oxygen (1 l/min). A ~1cm incision was made in the skin on the top of the head, and a 1mm hole drilled 2mm posterior to the junction of sagittal and coronal sutures of the skull (bregma) and 1mm lateral to the midline using a surgical bone microdrill (Harvard Apparatus, Edenbridge, UK). Cell suspension (5 μ l) was then injected at a depth of 3mm from the dura, at a rate of 2 μ l/min, using a 10 μ l syringe (VWR International, Lutterworth, UK) and a nanomite syringe pump (Harvard Apparatus). The needle was removed 3 minutes after completion of the injection and the skin repaired with Vetbond™ Tissue Adhesive (3M Animal Care Products, St Paul, MN, USA). Tumor establishment and growth were monitored with bioluminescence

imaging using a Xenogen IVIS[®] 200 system coupled with LivingImage software (Caliper Life Sciences, Runcorn, UK). Luciferin (150mg/kg, Caliper Life Sciences) was administered intraperitoneally 10 minutes before imaging. Total photon flux was established for automatically drawn ROIs at a constant threshold. MRE was performed when the photon flux reached a threshold value previously determined to represent a tumor of approximately 30-40mm³, a volume considered of sufficient size to acquire MRE data but not large enough to cause neurological effects in the mice. The average time from implantation to imaging was 18 days for the U-87 MG and MDA-MB-231 tumors and 22 days for the RG2 tumors.

Magnetic Resonance Elastography

All MRI studies were performed on a 7T Bruker horizontal bore MicroImaging system (Bruker Instruments, Ettlingen, Germany) using a 3cm birdcage volume coil. Anesthesia was induced by an intraperitoneal 10ml/kg injection of a combination of fentanyl citrate (0.315mg/ml) plus fluanisone (10mg/ml) (Hypnorm, Janssen Pharmaceutical, Oxford, UK) and midazolam (5mg/ml) (Roche, Welwyn Garden City, UK) and water (1:1:2). Core body temperature was maintained at ~37°C with warm air blown through the magnet bore.

MRE was performed as recently described (16). The mechanical vibrations were generated by an electromagnetic shaker (Brüel & Kjaer, Nærum, Denmark), and were transmitted through a flexible nylon rod to a square semi-curved piston positioned on the mouse head within the volume coil at the isocenter of the magnetic field (Supplementary Figure S1). Anatomical T₂-weighted images (using a rapid acquisition with refocused echoes (RARE) sequence, with TE = 36ms, TR = 4.5s, RARE factor = 8, 40 contiguous 1mm thick transverse slices, 1 average, matrix size 128×128 over a 3×3cm² field of view) covering the whole brain were used for determining tumor volumes, planning of the MRE acquisition, and optimisation of the local field homogeneity over the region of interest using the FASTMAP algorithm. MRE was performed using mechanical excitations at a vibration frequency of 1000 Hz, which generates mechanical waves inside the tumor with amplitude greater than 0.5μm. A 2D spin-echo sequence was modified with sinusoidal motion-sensitizing gradients synchronized to the mechanical excitation. Data were acquired in three orthogonal directions, from ten contiguous transverse slices (300μm thick), using 2 averages of 64 phase encoding steps over a 1.92×1.92cm² FOV, with TE = 27ms, TR = 1001ms and 8 time sampling steps, giving an isotropic spatial sampling of 300×300×300μm³ of the mechanical wave propagation displacement inside the tumor. The total acquisition time was ~ 51min. High resolution anatomical T₂-weighted images were subsequently acquired from the same ten contiguous transverse slices, (using a RARE sequence, with TE = 36ms, TR = 4.5s, RARE factor = 8, 300μm thick, 10 averages, matrix size 128×128 over a 1.92×1.92cm² field of view)

Image Reconstruction and Analysis

Parametric maps of the absolute value of the complex shear modulus $|G^*|$, elasticity G_d and viscosity G_1 (where $G^* = G_d + iG_1$) were reconstructed using an in-house software from the three-dimensional displacement vector measured as described above, and using the following equation (17):

$$-\rho\omega^2\vec{q}=G^*\nabla^2\vec{q}, \vec{q}=\vec{\nabla}\times\vec{u}\in C^3,$$

where \vec{q} is the complex-valued curl of the measured displacement field \vec{u} , ρ is the density of the material and ω is the angular frequency. For each slice, G_d and G_1 (kPa) were determined pixelwise from a region of interest (ROI) covering the whole tumor identified from T_2 -weighted images.

Histological Analysis

Tissue sections (5 μ m) were cut from tumor bearing brains that had been formalin-fixed and paraffin-embedded (FFPE). FFPE sections were stained with hematoxylin and eosin (H&E), visualized by light microscopy, then blind reviewed and scored by an experienced pathologist (S.P.) for in vasive growth, the presence of necrosis, edema and hemorrhage. Cellular density was also assessed on sections from two levels through each tumor, by counting the number of nuclei in four square ROIs from a total area of 0.01 mm² per field (x200 magnification, three or more fields assessed per section) (18). Collagen I and III were detected on adjacent FFPE tissue sections using picrosirius red staining (Supplementary Methods and Materials). In addition, collagen IV expression was detected by immunohistochemistry (rabbit polyclonal antibodies, ab6586, Abcam, Cambridge, UK). Microvessel density was assessed on FFPE sections stained for the murine vascular endothelial marker CD31 (rabbit EP3095, Millipore, Watford, UK). The number of vessels in four or five random fields of a total area assessed of 0.015 mm² each (x200 magnification). Luxol fast blue staining was also used to assess myelin fibers in adjacent sections (Supplementary Methods and Materials).

Statistical Analysis

Statistical analysis was performed with GraphPad Prism 6 (GraphPad Software Inc., La Jolla, USA). The mean of median values for all the quantitative MRE parameters, the mean values for tumor volume, cellular density and microvessel density were used for statistical analysis. Any significant differences in quantitative MRE parameters were identified using the non-parametric Mann-Whitney U test, with a 5% level of significance. Any significant differences in tumour volume and quantitative histopathological parameters were identified using Student's 2-tailed unpaired t-test, with a 5% level of significance. Significant correlations between the mean values for all the quantitative MRE parameters and cellular and microvessel density were determined using linear regression analysis, confirmed by using the robust regression and outlier removal approach (19).

Results

Intracranially implanted U-87 MG, RG2 and MDA-MB-231 tumors are softer and less viscous than healthy brain parenchyma

Parametric maps of elasticity (G_d) and viscosity (G_1) revealed the symmetrical and characteristic anatomical structures of the healthy mouse brain, including the relatively stiffer corpus callosum and the softer thalamus (Figure 1). In mouse brains bearing tumors

derived from U-87 MG, RG2 or MDA-MB-231 cells, both elasticity and viscosity maps showed pronounced contrast between the established tumor (mean tumor volume $35 \pm 3 \text{ mm}^3$) and the surrounding brain, based on viscoelastic image appearances and on analyses within regions of interest drawn using boundaries defined by the T_2 -weighted MR images (Figure 2, Supplementary Figure S2). The presence and location of the tumors were confirmed by H&E staining of FFPE tissue sections. Quantitative analysis of the elastic modulus G_d and the viscosity modulus G_l revealed that the three tumor types were significantly less elastic (G_d , U-87 MG: $4.80 \pm 0.21 \text{ kPa}$ > RG2: $4.22 \pm 0.14 \text{ kPa}$ > MDA-MB-231: $3.74 \pm 0.14 \text{ kPa}$) and viscous (G_l , U-87 MG: 2.94 ± 0.19 > RG2: $2.41 \pm 0.09 \text{ kPa}$ > MDA-MB-231: $2.21 \pm 0.07 \text{ kPa}$) than healthy brain parenchyma G_d , $5.89 \pm 0.17 \text{ kPa}$ and G_l , $4.36 \pm 0.17 \text{ kPa}$ (Figure 3A and B). Histogram analysis demonstrated a clear shift in the distribution of G_d and G_l values in the tumor compared with healthy brain tissue (Figure 3C and D). In the majority of mice with tumors, the lateral ventricles were markedly dilated and demonstrated low elasticity and viscosity (Figure 1).

Intracranially implanted U-87 MG, RG2 and MDA-MB-231 tumors have different viscoelastic properties

Significantly different values of G_d were determined across the three tumor models, with tumors derived from U-87 MG cells being the stiffest and tumors derived from MDA-MB-231 the softest (Figures 3A & C). A similarly significant trend was also found for G_l , with tumors derived from U-87 MG cells significantly more viscous than tumors derived from either RG2 or MDA-MB-231 cells (Figures 3B & D).

Cellular and microvessel density contribute to the relative stiffness of intracranially implanted brain tumors

Table 1 summarizes the histopathological features of each tumor model. Markedly different growth patterns were apparent, with tumors derived from U-87 MG cells being well-circumscribed with sparse foci of infiltrative cells, whilst tumors derived from MDA-MB-231 cells were substantially more infiltrative (Figure 4). Tumors derived from U-87 MG and RG2 cells had a homogeneous dense cellularity, whereas tumors derived from MDA-MB-231 cells presented with regions of sparse cell density and edema. Quantitative analysis confirmed a significantly lower cellular density in tumors derived from MDA-MB-231 cells compared with tumors derived from U-87 MG or RG2 cells (Figure 5A). At the time of imaging or excision, no areas of gross necrosis were detected in any of the tumor models.

Myelin was only detected as sparse and very fine fibers within tumors derived from U-87 MG cells. Myelin fibers were also detected at the invasive margin of all tumors in the myelinated structures of the brain that were being invaded (Supplementary Figure S3). Type I, III and IV collagen were more abundant in tumor compared with brain parenchyma, but were mainly localized to the basement membrane of the vasculature in all tumor types. There was no difference in collagen content between the tumor types. The three models demonstrated significantly different microvessel density (MVD) as measured on CD31-stained FFPE tissue sections of the MRE-imaged mice, with the highest vessel density in U-87 MG tumors and the lowest score in MDA-MB-231 tumors (Figures 4 & 5B).

Microvessel density was significantly lower in normal brain parenchyma compared with U-87 MG and RG2 tumors (* $p < 0.05$).

The functional vascular phenotype of the three tumor models was also investigated in separate cohorts using the perfusion marker Hoechst 33342 (see Supplementary Materials and Methods). Fluorescence microscopy of Hoechst 33342 uptake revealed no significant difference in the degree of functionally perfused vasculature (Supplementary Figures S4A & B). However, subsequent processing and quantitative analysis of CD31 immunofluorescence on the same frozen tissue sections corroborated the CD31 MVD data acquired on FFPE sections of the imaged tumors (Supplementary Figures S4 A & C).

Linear regression analysis revealed significant positive correlations between tumor cellular density and MVD with both elasticity G_d ($r=0.61$, $p=0.01$ and $r=0.54$, $p=0.03$ respectively), and viscosity G_1 ($r=0.57$, $p=0.02$ and $r=0.48$, $p=0.07$ respectively) (Figures 5C & D).

Discussion

It is well established that increased tissue rigidity in extracranial tumors is associated with an invasive phenotype, and can influence therapeutic response (3). Reciprocally, therapeutic prevention of tissue stiffening is predicted to impede cancer progression and metastasis, and drugs targeting the mechanical properties of the extracellular matrix are being developed (4,20-22). In this setting, the ability of MRE to non-invasively quantify tumor mechanical properties is being actively exploited and should prove beneficial for cancer diagnosis, prognosis and for monitoring response to these novel therapeutics (23,24).

Using MRE, we have shown that three intracranially implanted tumors derived from U-87 MG human glioma, RG2 rat glioma or MDA-MB-231 metastatic human breast carcinoma cells, which present with different growth patterns were all significantly softer than the surrounding brain tissue *in vivo*. Given the well-described association of increased stiffness with malignancy in, for example, breast or liver cancer (23), the relative softness of these intracranially implanted tumor models compared with normal brain was initially unexpected. However, this observation is consistent with the reported soft consistency of brain malignancies, based on pathological examination or intra-operative assessment (25-27). In a recent clinical prospective study, preliminary evidence of the relative softness of malignant primary brain tumors and metastases with a range of differentiation status and grade was provided by MRE (12).

In interrogating the pathological determinants underpinning our MRE data we have demonstrated that both cellular density and MVD contribute to the relative stiffness of these soft brain tumor models. More generally, cellular architecture (cellular arrangement, size, shape and density), the vascular network and its collagen-supported scaffold are major structural components of the tumor microenvironment, and as such represent important determinants of the intrinsic stiffness of tumors. This is corroborated by recent MRE studies showing a decrease in the magnitude of the shear modulus (G^*) upon therapy-induced necrosis or a decrease in MVD, and the correlation between increased G^* and MVD upon progression in *in vivo* models of colon cancer and lymphoma (28-30).

These pathological correlates, however, do not explain the softness of brain tumors. The ECM is another major contributor to the viscoelastic properties of tumors. Breast cancer cells have been shown to be more compliant (softer) than their non-malignant counterparts (31), yet malignant breast tumors are stiff due to their ECM, being rich in cross-linked collagen fibers (32). In contrast, the ECM of brain tumors has been shown to share the unique composition of that of the healthy brain, characterized by high concentrations of hyaluronic acid and the absence of fibrillar networks such as collagen, fibronectin and vitronectin, or basement membrane proteins such as laminin, which are only found in the vascular or perivascular space (33). The unique composition of the ECM contributes to making brain the softest tissue in the human body (34). The lower viscoelastic properties of brain tumors relative to the brain parenchyma itself may be attributed to the absence of structural anisotropy due to the rapid and chaotic tumor cell growth, which contrast with the highly networked and organized microstructure of brain tissue. The heterogeneous and symmetrical distribution of mechanical properties in the healthy brain, observed in our study, correlate with the regional differences in the microstructure and organization of the brain parenchyma (35). For example, the elevated viscoelasticity associated with the corpus callosum, a compact bundle of myelin-sheathed axonal projections connecting the two brain hemispheres, is a prime example of the direct relationship between increased organization and increased stiffness in the brain. In contrast, the lower stiffness observed in the dilated ventricles in tumor-bearing mice is a consequence of the inability of cerebrospinal fluid to withstand a shear stress (36).

Our histopathologically-correlated MRE data provide further *in vivo* evidence of the sensitivity of MRE-measured viscoelastic properties for changes in tissue microstructure at scales that are far below the resolution of the MR images (37,38), demonstrated here for the first time in brain tumors. This is consistent with the predictions of models for the mechanical properties of networked microstructures which have been shown to scale into unique macroscopic mechanical signatures (39), making MRE a very promising methodology for the detection and differential diagnosis of malignancies (37), as illustrated herein by the discrimination of the three intracranial tumor models based on their differential mechanical phenotypes.

MRE is already in use clinically for the staging of liver fibrosis and the differential diagnosis of malignant nodules in breast, liver and prostate cancer (23,40-42). Having overcome the challenges of transmitting waves through the human cranium, MRE has also been successfully implemented for the routine examination of neurology patients including those with brain malignancies (9,11,12), and shown to detect changes in brain tissue integrity associated with several neurological disorders, including multiple sclerosis (MS) (43,44). The potential use of MRE in pre-operative planning in patients with meningioma, in which the complexity of surgical resection increases with tumor stiffness, has been recently highlighted (45).

The ability of MRE to assist in the delineation of brain tumors for preoperative management is also being actively investigated. The provision of strong conclusions on the accuracy of tumor delineation on our viscoelastic maps is challenging, as nonlinear deformations occurring during tissue processing preclude the use of H&E-stained sections as a gold

standard to define tumor boundaries. Further *in vivo* studies co-registering MRE-acquired viscoelastic maps with images acquired with techniques such as stimulated Raman scattering (SRS) microscopy, shown to accurately delineate tumors in orthotopic models of human gliomas both *in situ* and *ex vivo* using fresh tissue slices (46), would provide definitive conclusions on the utility of MRE to delineate brain tumors.

In conclusion, our pre-clinical study provides definitive evidence for the relative softness of intracranial tumors *in vivo*. In addition to measuring stiffness, we demonstrate that MRE is sensitive to changes in intracranially implanted tumor microstructure, including those within the cellular and vascular networks, allowing the discrimination of three phenotypically different tumor models based on their different mechanical properties. Our study thus supports further evaluation of clinical MRE for the detection and differential diagnosis of brain tumors (or metastases) and reinforces MRE as a promising and attractive addition to the multi-parametric diagnostic neuroimaging methodologies, which already play a crucial role in the management of patients with brain malignancies (47).

Supplementary Material

Refer to Web version on PubMed Central for supplementary material.

Acknowledgments

Financial support: We acknowledge support from The Institute of Cancer Research Cancer Research UK and EPSRC Cancer Imaging Centre, in association with the MRC and Department of Health (England) grant C1060/A10334, NHS funding to the NIHR Biomedical Research Centre, Cancer Research UK funding to the Cancer Therapeutics Unit grant C309/A11566, the Department of Health via the National Institute for Health Research (NIHR) comprehensive Biomedical Research Centre award to Guy's & St Thomas' NHS Foundation Trust in partnership with King's College London and King's College Hospital NHS Foundation Trust, The Wellcome Trust grant #091763Z/10/Z, EPSRC Platform Grant #EP/H046526/1, and a Paul O'Gorman Postdoctoral Fellowship funded by Children with Cancer UK (Y.J.), a Dorothy Hodgkin Postgraduate Award (DHPA) #EP/P505828/1 (J.L.), and AstraZeneca.

References

1. Netti PA, Berk DA, Swartz MA, Grodzinsky AJ, Jain RK. Role of extracellular matrix assembly in interstitial transport in solid tumors. *Cancer Res.* 2000; 60:2497–2503. [PubMed: 10811131]
2. Akiri G, Sabo E, Dafni H, et al. Lysyl oxidase-related protein-1 promotes tumor fibrosis and tumor progression *in vivo*. *Cancer Res.* 2003; 63:1657–1666. [PubMed: 12670920]
3. Butcher DT, Alliston T, Weaver VM. A tense situation: forcing tumour progression. *Nat Rev Cancer.* 2009; 9:108–122. [PubMed: 19165226]
4. Paszek MJ, Zahir N, Johnson KR, et al. Tensional homeostasis and the malignant phenotype. *Cancer Cell.* 2005; 8:241–254. [PubMed: 16169468]
5. Mouw JK, Yui Y, Damiano L, et al. Tissue mechanics modulate microRNA-dependent PTEN expression to regulate malignant progression. *Nat Med.* 2014; 20:360–367. [PubMed: 24633304]
6. Lu P, Weaver VM, Werb Z. The extracellular matrix: a dynamic niche in cancer progression. *J Cell Biol.* 2012; 196:395–406. [PubMed: 22351925]
7. Cox TR, Ertler JT. Remodeling and homeostasis of the extracellular matrix: implications for fibrotic diseases and cancer. *Dis Model Mech.* 2011; 4:165–178. [PubMed: 21324931]
8. Muthupillai R, Lomas DJ, Rossman PJ, Greenleaf JF, Manduca A, Ehman RL. Magnetic resonance elastography by direct visualization of propagating acoustic strain waves. *Science.* 1995; 269:1854–1857. [PubMed: 7569924]

9. Green MA, Bilston LE, Sinkus R. In vivo brain viscoelastic properties measured by magnetic resonance elastography. *NMR Biomed.* 2008; 21:755–764. [PubMed: 18457350]
10. Kruse SA, Rose GH, Glaser KJ, et al. Magnetic resonance elastography of the brain. *NeuroImage.* 2008; 39:231–237. [PubMed: 17913514]
11. Sack I, Beierbach B, Hamhaber U, Klatt D, Braun J. Non-invasive measurement of brain viscoelasticity using magnetic resonance elastography. *NMR Biomed.* 2008; 21:265–271. [PubMed: 17614101]
12. Simon M, Guo J, Papazoglou S, et al. Non-invasive characterization of intracranial tumors by magnetic resonance elastography. *New J Physics.* 2013; 15:085024.
13. Munoz R, Man S, Shaked Y, et al. Highly efficacious nontoxic preclinical treatment for advanced metastatic breast cancer using combination oral UFT-cyclophosphamide metronomic chemotherapy. *Cancer Res.* 2006; 66:3386–3391. [PubMed: 16585158]
14. Workman P, Aboagye E, Balkwill F, et al. Guidelines for the welfare and use of animals in cancer research. *Br J Cancer.* 2010; 102:1555–1577. [PubMed: 20502460]
15. Kilkeny C, Browne WJ, Cuthill IC, Emerson M, Altman DG. Improving bioscience research reporting: the ARRIVE guidelines for reporting animal research. *PLoS Biol.* 2010; 8:e1000412. [PubMed: 20613859]
16. Li J, Jamin Y, Boulton JK, et al. Tumour biomechanical response to the vascular disrupting agent ZD6126 in vivo assessed by magnetic resonance elastography. *Brit J Cancer.* 2014 In Press.
17. Sinkus R, Siegmann K, Xydeas T, Tanter M, Claussen C, Fink M. MR elastography of breast lesions: understanding the solid/liquid duality can improve the specificity of contrast-enhanced MR mammography. *Magn Reson Med.* 2007; 58:1135–1144. [PubMed: 17969009]
18. Schnapauff D, Zeile M, Niederhagen MB, et al. Diffusion-weighted echo-planar magnetic resonance imaging for the assessment of tumor cellularity in patients with soft-tissue sarcomas. *J Magn Reson Imaging.* 2009; 29:1355–1359. [PubMed: 19472392]
19. Motulsky HJ, Brown RE. Detecting outliers when fitting data with nonlinear regression - a new method based on robust nonlinear regression and the false discovery rate. *BMC Bioinformatics.* 2006; 7:123. [PubMed: 16526949]
20. Cox TR, Bird D, Baker AM, et al. LOX-mediated collagen crosslinking is responsible for fibrosis-enhanced metastasis. *Cancer Res.* 2013; 73:1721–1732. [PubMed: 23345161]
21. Erler JT, Bennewith KL, Nicolau M, et al. Lysyl oxidase is essential for hypoxia-induced metastasis. *Nature.* 2006; 440:1222–1226. [PubMed: 16642001]
22. Baker AM, Bird D, Lang G, Cox TR, Erler JT. Lysyl oxidase enzymatic function increases stiffness to drive colorectal cancer progression through FAK. *Oncogene.* 2013; 32:1863–1868. [PubMed: 22641216]
23. Garteiser P, Doblaz S, Daire JL, et al. MR elastography of liver tumours: value of viscoelastic properties for tumour characterisation. *Eur Radiol.* 2012; 22:2169–2177. [PubMed: 22572989]
24. Sinkus R, Tanter M, Xydeas T, Catheline S, Bercoff J, Fink M. Viscoelastic shear properties of in vivo breast lesions measured by MR elastography. *Magn Reson Imaging.* 2005; 23:159–165. [PubMed: 15833607]
25. Jones H, Steart PV, Weller RO. Spindle-cell glioblastoma or gliosarcoma? *Neuropath Appl Neuro.* 1991; 17:177–187.
26. Suzuki Y, Sugimoto T, Shibuya M, Sugita K, Patel SJ. Meningiomas: correlation between MRI characteristics and operative findings including consistency. *Acta Neurochirurgica.* 1994; 129:39–46. [PubMed: 7998494]
27. Aas AT, Brun A, Blennow C, Stromblad S, Salford LG. The RG2 rat glioma model. *J Neurooncol.* 1995; 23:175–183. [PubMed: 7673979]
28. Juge L, Doan BT, Seguin J, et al. Colon tumor growth and antivascular treatment in mice: complementary assessment with MR elastography and diffusion-weighted MR imaging. *Radiology.* 2012; 264:436–444. [PubMed: 22692038]
29. Li J, Jamin Y, Boulton JK, et al. Tumour biomechanical response to the vascular disrupting agent ZD6126 in vivo assessed by magnetic resonance elastography. *Br J Cancer.* 2014; 110:1727–1732. [PubMed: 24569471]

30. Pepin KM, Chen J, Glaser KJ, et al. MR elastography derived shear stiffness—a new imaging biomarker for the assessment of early tumor response to chemotherapy. *Magn Reson Med*. 2013; 71:1834–1840. [PubMed: 23801372]
31. Swaminathan V, Mythreya K, O'Brien ET, Berchuck A, Blobe GC, Superfine R. Mechanical stiffness grades metastatic potential in patient tumor cells and in cancer cell lines. *Cancer Res*. 2011; 71:5075–5080. [PubMed: 21642375]
32. Levental KR, Yu H, Kass L, et al. Matrix crosslinking forces tumor progression by enhancing integrin signaling. *Cell*. 2009; 139:891–906. [PubMed: 19931152]
33. Bellail AC, Hunter SB, Brat DJ, Tan C, Van Meir EG. Microregional extracellular matrix heterogeneity in brain modulates glioma cell invasion. *Int J Biochem Cell Biol*. 2004; 36:1046–1069. [PubMed: 15094120]
34. Bilston, LE. Brain Tissue Mechanical Properties. In: Bilston, LE., editor. *Neural Tissue Biomechanics*. Springer; Berlin Heidelberg; 2011. p. 11-24.
35. Guo J, Hirsch S, Fehlner A, et al. Towards an elastographic atlas of brain anatomy. *Plos One*. 2013; 8:e71807. [PubMed: 23977148]
36. Pattison AJ, Lollis SS, Perrinez PR, et al. Time-harmonic magnetic resonance elastography of the normal feline brain. *J Biomech*. 2010; 43:2747–2752. [PubMed: 20655045]
37. Sack I, Johrens K, Wurfel J, Braun J. Structure-sensitive elastography: on the viscoelastic powerlaw behavior of in vivo human tissue in health and disease. *Soft matter*. 2013; 9:5672–5680.
38. Schregel K, Wuerfel Nee Tysiak E, Garteiser P, et al. Demyelination reduces brain parenchymal stiffness quantified in vivo by magnetic resonance elastography. *Proc Natl Acad Sci U S A*. 2012; 109:6650–6655. [PubMed: 22492966]
39. Guo J, Posnansky O, Hirsch S, et al. Fractal network dimension and viscoelastic powerlaw behavior: II. An experimental study of structure-mimicking phantoms by magnetic resonance elastography. *Phys Med Biol*. 2012; 57:4041. [PubMed: 22674199]
40. Huwart L, Sempoux C, Vicaut E, et al. Magnetic resonance elastography for the noninvasive staging of liver fibrosis. *Gastroenterology*. 2008; 135:32–40. [PubMed: 18471441]
41. Xydeas T, Siegmann K, Sinkus R, Krainick-Strobel U, Miller S, Claussen CD. Magnetic resonance elastography of the breast: correlation of signal intensity data with viscoelastic properties. *Invest Radiol*. 2005; 40:412–420. [PubMed: 15973132]
42. Sahebjavaher RS, Frew S, Bylinskii A, et al. Prostate MR elastography with transperineal electromagnetic actuation and a fast fractionally encoded steady-state gradient echo sequence. *NMR Biomed*. 2014; 27:784–794. [PubMed: 24764278]
43. Wuerfel J, Paul F, Beierbach B, et al. MR-elastography reveals degradation of tissue integrity in multiple sclerosis. *NeuroImage*. 2010; 49:2520–2525. [PubMed: 19539039]
44. Freimann FB, Streitberger KJ, Klatt D, et al. Alteration of brain viscoelasticity after shunt treatment in normal pressure hydrocephalus. *Neuroradiol*. 2012; 54:189–196.
45. Murphy MC, Huston J 3rd, Glaser KJ, et al. Preoperative assessment of meningioma stiffness using magnetic resonance elastography. *J Neurosurg*. 2013; 118:643–648. [PubMed: 23082888]
46. Ji M, Orringer DA, Freudiger CW, et al. Rapid, label-free detection of brain tumors with stimulated Raman scattering microscopy. *Science Transl Med*. 2013; 5:201ra119.
47. Essig M, Anzalone N, Combs SE, et al. MR imaging of neoplastic central nervous system lesions: review and recommendations for current practice. *Am J Neuroradiol*. 2012; 33:803–817. [PubMed: 22016411]

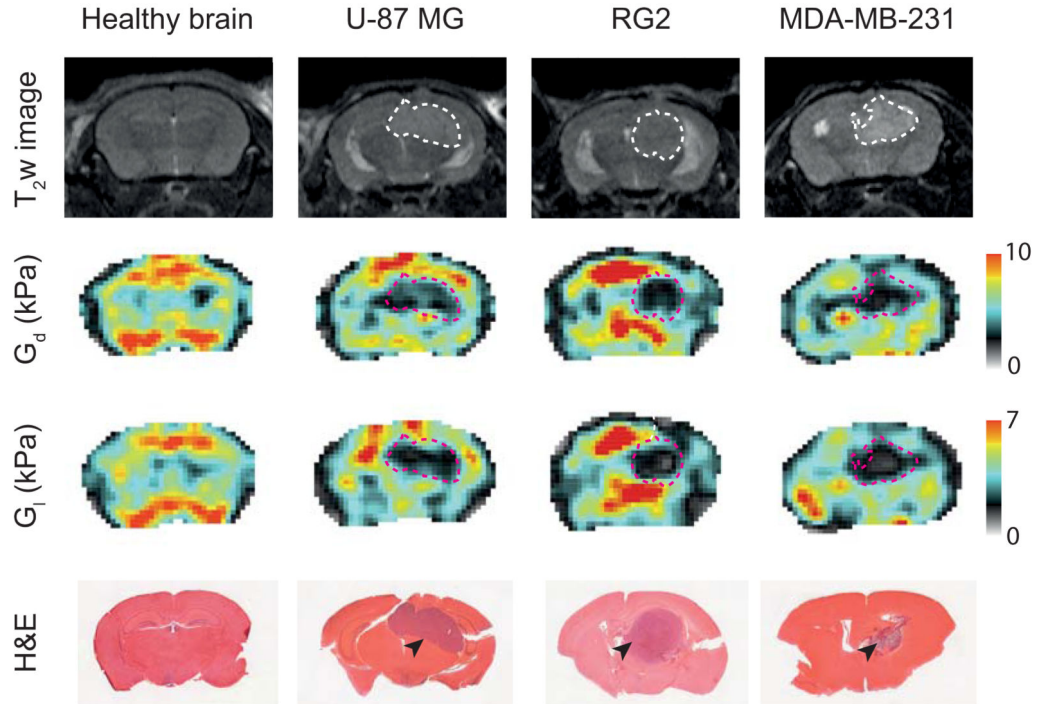


Figure 1.

Non-invasive imaging of the viscoelastic properties of intracranial tumors assessed by magnetic resonance elastography (MRE). Anatomical T₂-weighted MR images, and parametric maps of elasticity (G_d) and viscosity (G_l), acquired from a non-tumor bearing mouse, and mice bearing tumors derived from human adult U-87 MG glioblastoma, *N*-ethyl-*N*-nitrosourea-induced RG2 rat glioma, or human triple negative MDA-MB-231 breast carcinoma cells are shown. (---) indicates the tumor boundaries defined on T₂-weighted images. Images of whole hematoxylin and eosin stained sections obtained from the same mice are also shown, with the tumor location arrowed.

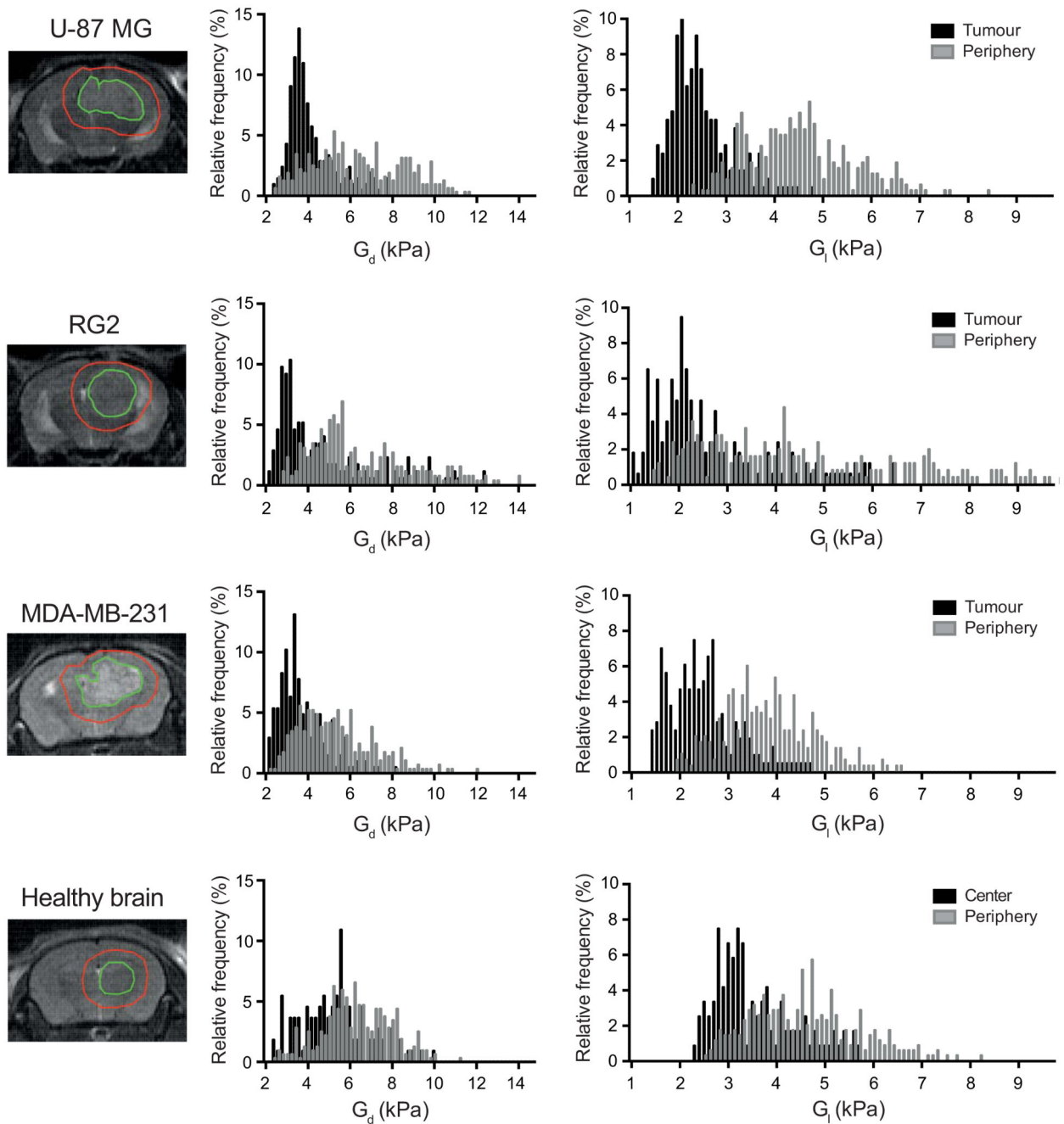


Figure 2.

Frequency histograms showing the distribution of elasticity (G_d) and viscosity (G_1) and in tumours and their periphery, in representative mice bearing intracranially implanted U-87 MG, RG2, or MDA-MB-231 tumors. Tumor regions of interest were defined on T₂-weighted images. Histogram analysis was also performed in the brain of a control healthy mouse.

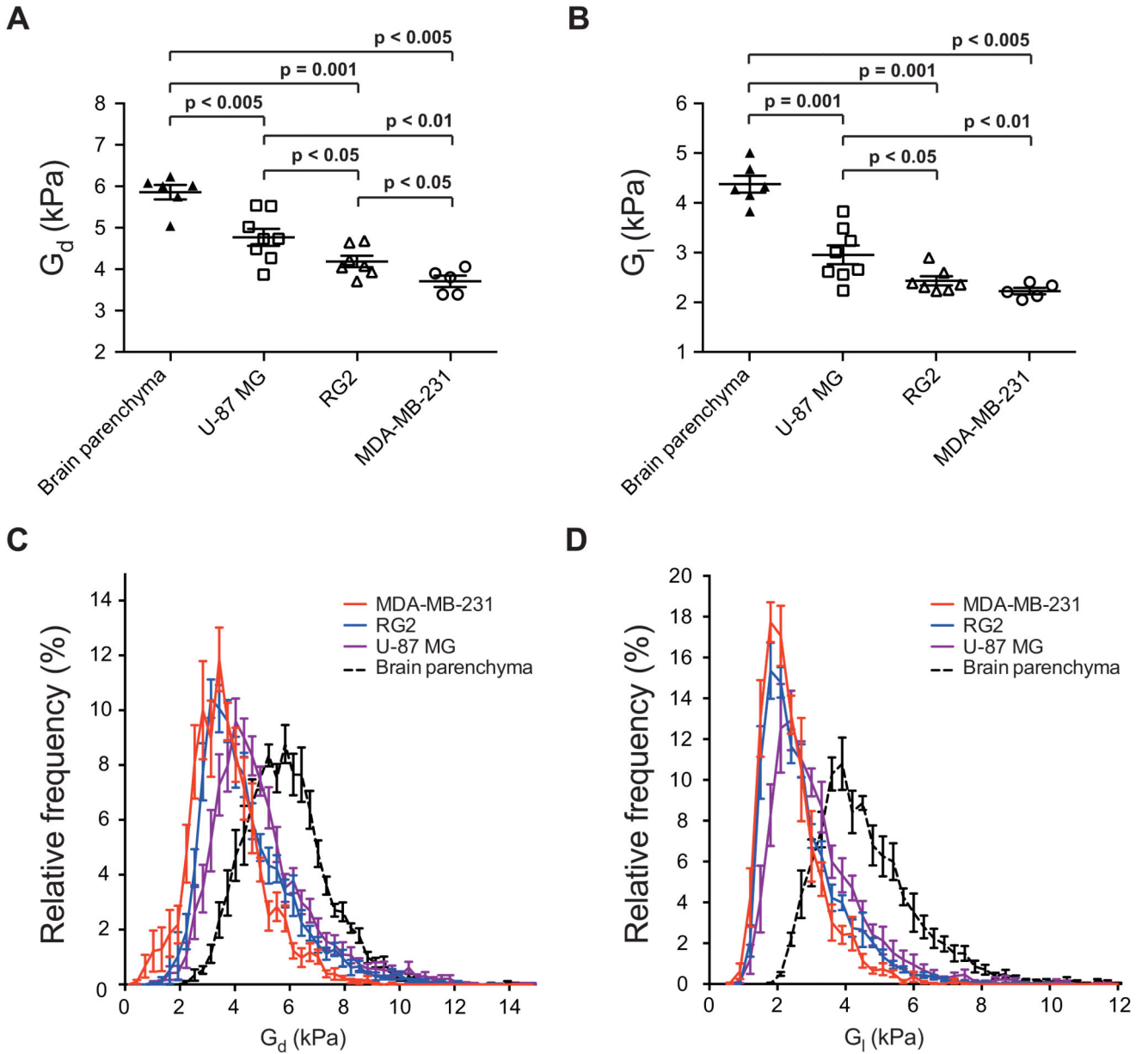


Figure 3. Quantitative assessment of A) elasticity (G_d) and B) viscosity (G_1), determined *in vivo* from healthy brain parenchyma in control mice (n=6), and intracranially implanted U-87 MG (n=8), RG2 (n=7) and MDA-MB-231 (n=5) tumors, using magnetic resonance elastography. Data are presented as the median values for each tumor, and as the mean \pm 1 s.e.m. across each cohort. Significance testing employed Mann-Whitney *U* test with a 5% level of significance. The associated frequency histograms showing the distribution of C) elasticity (G_d) and D) viscosity (G_1) for brain parenchyma and the three tumor types are also shown.

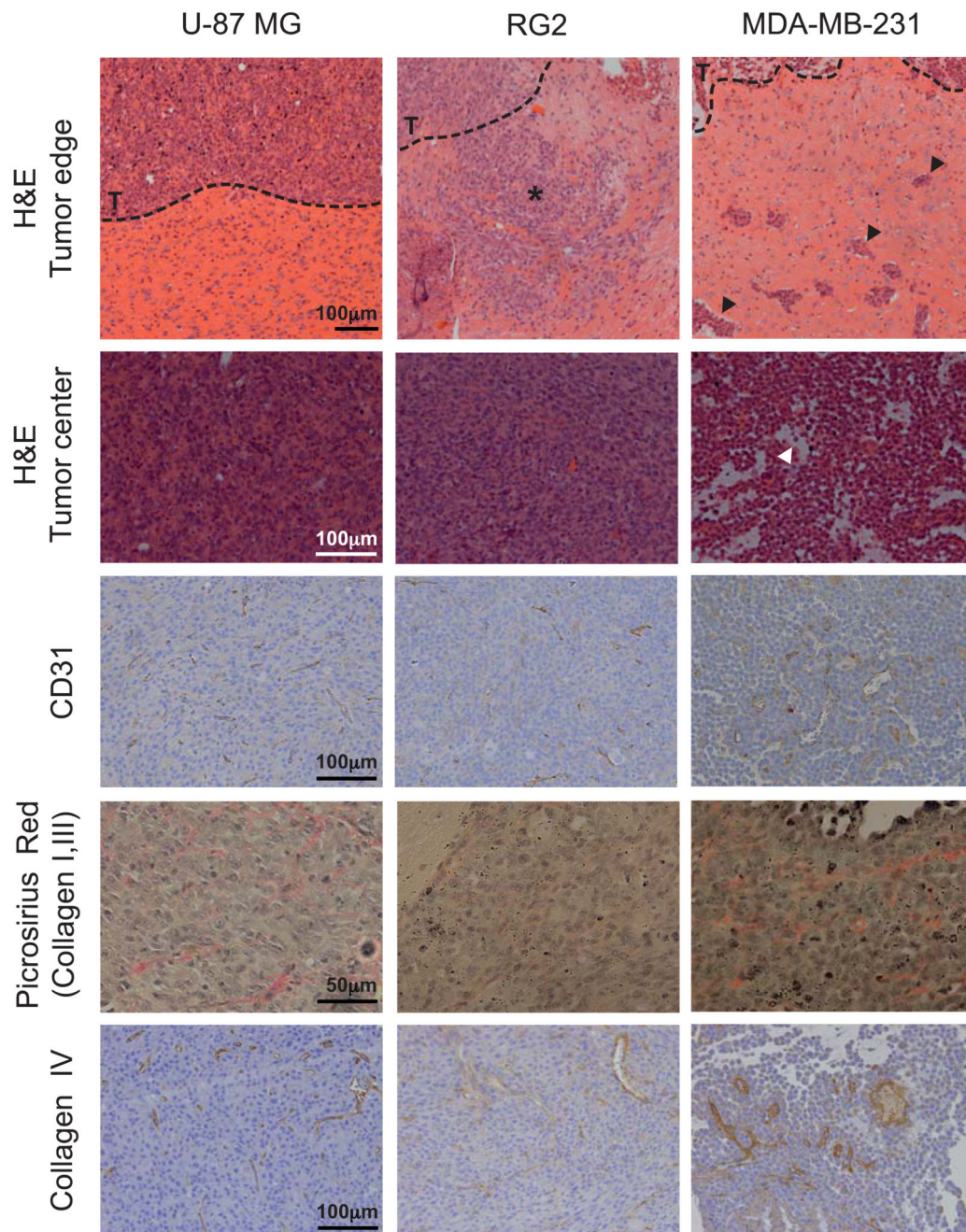


Figure 4. Histopathology of intracranially implanted U-87 MG, RG2 and MDA-MB-231 tumors. Note the different infiltrative patterns at the tumor boundary (--- T) between the RG2 (*) and MDA-MB-231 (arrowed) tumors. Also note the presence of edema evident on H&E stained sections (arrowed, white), and large distended vessels as shown by immunohistochemical staining for the murine vascular endothelial marker CD31, in the MDA-MB-231 tumor.

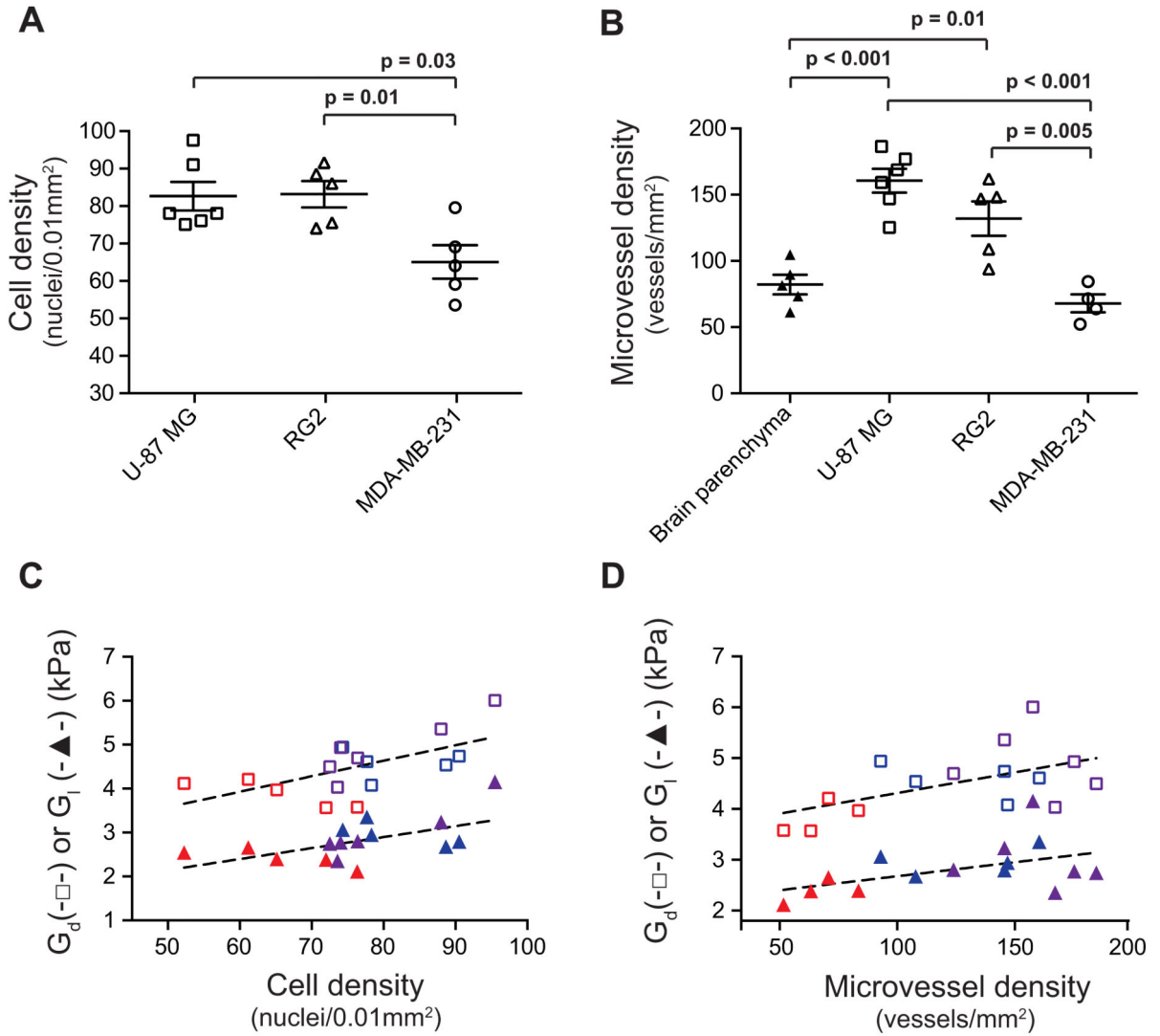


Figure 5. Quantitative histological assessment of A) cell density and B) microvessel density, determined from intracranially implanted U-87 MG (n=6), RG2 (n=5) and MDA-MB-231 (n=5) tumors. Microvessel density was also quantified in healthy brain parenchyma in control mice (n=6). Data are presented as the median values for each tumor, and as the mean \pm 1 s.e.m. across each cohort. Significance testing employed Student's two-tailed unpaired t-tests with a 5% level of significance. The relationship of MR elastography-derived elasticity (G_d) and viscosity (G_l) with C) cell density ($r=0.61$, $p=0.01$ and $r=0.57$, $p=0.02$ respectively), and D) microvessel density ($r=0.54$, $p=0.03$ and $r=0.48$, $p=0.07$ respectively) across all the intracranially implanted tumors is shown (□,▲: U-87 MG, □,▲: RG2, □,▲: MDA-MB-231).

Table 1

Summary of the histopathological features of tumors derived from adult human U-87 MG glioblastoma cells, *N*-ethyl-*N*-nitrosourea-induced rat RG2 glioma cells, or human triple negative MDA-MB-231 breast carcinoma cells implanted intracranially in athymic mice (n=3 per tumor type).

	M	Growth pattern	Cellularity	Necrosis	Edema	Hemorrhage	Myelin fibres
U-87 MG	1	Well circumscribed Presence of infiltrative foci	Dense	-	-	Small foci	Foci of very fine fibers in the centre
	2	Well circumscribed Presence of infiltrative foci	Dense	-	-	-	Foci of cells infiltrating highly myelinated part of the brain
	3	Well circumscribed Presence of infiltrative foci	Dense	-	-	-	Few, very fine fibres within the tumor
RG2	1	Moderately infiltrative	Dense	-	-	+ (center)	Fine fiber are seen between tumor islands at the periphery
	2	Moderately infiltrative	Dense	-	-	-	-
	3	Moderately infiltrative	Dense	-	-	-	Infiltrative part of the tumor contains entrapped highly myelinated structures
MDA-MB-231	1	Highly infiltrative	Dense at the periphery Loose texture in centre	-	+ (center)	+ (center)	Infiltrative margin is intermixed with moderately myelinated structures of normal brain
	2	Highly infiltrative	Dense at the periphery Loose texture in centre	-	+ (center)	-	Infiltrative margin is intermixed with moderately and highly myelinated structures of normal brain
	3	Highly infiltrative	Heterogeneous	-	+	-	Infiltrative margin is intermixed with well-myelinated structures of normal brain